The Affects of Ce Doping Cr$_2$O$_3$ Based Catalysts Supported on Activated Carbon for 1,2-Dichloroethane Abatement

Tabet Tsiankoraka Ahmadaly Adam [a*], Pengfei Zhu [a], Na Li [a], Zhaoxia Hu [a] and Shouwen Chen [a*]

[a] *School of Environmental and Biological Engineering, Nanjing University of Science and Technology, Nanjing-210094, PR, China.*

Authors' contributions

This work was carried out in collaboration among all authors. Authors TTAA and SC designed the study. Author TTAA performed the statistical analysis, wrote the protocol, and first draft of the manuscript. Author PZ managed the analyses of the study. Authors NL and ZH managed the literature searches. All authors read and approved the final manuscript.

Original Research Article

ABSTRACT

Hydrothermal method is used to prepare activated carbon (AC) supported chromium-based catalysts for the catalytic combustion of 1,2-dichloroethane (DCE). The physicochemical properties relating catalysts are evaluated by several characterization techniques such as XRD, SEM, XPS, N$_2$ adsorption-desorption isotherms, H$_2$-TPR and NH$_3$-TPR. The outcomes demonstrated that the Cr$_2$O$_3$ is the perfect targeted base catalyst

_____

Corresponding author: Email: babalytabet@gmail.com, chensw@njust.edu.cn;

adding to the facts that the hydrothermal approach is an appropriate way to create catalysts with superior properties. The textural characteristics, reducibility, and acidity of the Cr-based catalysts were all enhanced by the addition of cerium (Ce) and AC. Nevertheless, the research shows how crucial the Ce doping amount is for adjusting the physicochemical characteristics and catalytic efficacy of Cr-based catalysts. The catalyst 20Ce-Cr/AC has the maximum catalytic activity when it came to DCE combustion, where its T_{50} and T_{90} attaining of 247°C and 269.5°C, correspondingly. This is explained by the ideal Ce doping level, which improves the redox characteristics and revealed more active sites.

Keywords: Transition metals; Ce-Cr/AC; CeO_2-Cr_3O_4; catalytic performance; DCE oxidation; redox properties.

1. INTRODUCTION

Cl-containing volatile organic compounds (CVOCs) are one type of volatile organic compound (VOC) among others, which are far more hazardous and challenging to handle than regular VOCs [1,2]. They are released into the atmosphere and have the potential to negatively impact the ecosystem and human health, given their unusually high stability, endurance, and toxicity. When directly exposed to humans, these CVOCs can induce a variety of health effects, including cancer, and they can also have major photochemical interactions with other released pollutants, like SO_x and NO_x [1]. Regarded as a representative member of CVOCs, 1,2-dichloroethane (DCE) is extensively utilized in various manufacturing processes, including metal degreaser and industrial solvent [3]. As a result, it significantly contributes to photochemical smog, haze, and ozone layer depletion [4]. Due to their hazardous characteristics, strict laws implementing strict requirements on CVOC abatement systems are in place to regulate the emission of these toxic wastes.

Catalytic combustion is one technique that has been proposed for disposing these harmful chemicals, and it is quite effective in removing trace levels (<1%) of Cl-VOCs at low temperatures [5]. Because catalytic combustion is the preferred method, it has a better development prospect than high temperature combustion because of its low operating temperature, low energy consumption, and high selectivity to the most coveted and ecologically friendly products like CO_2, H_2O, and HCl [6]. The primary operational characteristic of this approach is choosing the appropriate catalyst while taking activity, durability, cost, and selectivity into account at the same time.

Currently, transition oxide and noble metal catalysts are the main topics of study for powder catalysts. Formerly, noble metals, particularly Pt and Pd have been used to high-surface area supports (γ-Al_2O_3, SiO_2, zeolites). The quest for more affordable and reliable substitutes has been spurred by their exorbitant expense and vulnerability to chlorine exposure, even though they exhibit noticeable activity in the oxidation of these contaminants [7]. Thus, transitional metal oxides, also known as rare earth oxides, are viewed as desirable alternatives. Examples of these oxides are Ce- [8–10], Co– [11], Mn– [12], and Cr– [13,14]. They are potentially very promising due to their inexpensive cost, accessibility, strong resistance to chlorine, remarkable reducibility, and thermal stability.

When it comes to the removal of different Cl-VOCs, Cr_2O_3 has one of the greatest levels of catalytic activity in contrast to other transition metal oxides [15–20]. However, these transition metal oxides may become somewhat deactivated when utilized as a single component due to the loss of active sites or the creation of volatile species at low temperatures. This could limit the applications of transition metal oxides. So, concern over Cr loss during the long-term reaction has restricted the practical applicability of its catalytic activity. For instance, a number of investigations have documented the irreversible deactivation brought by the volatile CrO_2Cl_2 that forms on the CrO_x/Al_2O_3 surface when active Cr components are lost [21,22]. Therefore, it is imperative to create novel catalysts for the oxidation of Cl-VOCs that are more stable and active. Additionally, more research should be done on the regeneration treatment and potential deactivation mechanism. Numerous strategies have been established to date to increase the structural flaws on metal oxide surfaces,

including etching procedures, metal doping, building high-index crystal planes, supporting, and so on.

In the past couple of years, CeO_2-based materials have been used as a support, main active element, or enhancer in many catalyst systems because of their outstanding redox properties, oxygen retention capacity, cost-effectiveness. and green credentials. They also exhibit substantial oxidative activity in the oxidation of CVOCs and good resistivity to Cl-poisoning [23]. All of these characteristics allow CeO_2 to undergo a rapid and reversible redox cycle of $Ce^{4+} \rightarrow Ce^{3+}$ at a comparatively low temperature [24–28]. When de Rivas et al. [23] looked into a variety of Ce/Zr mixed oxides for the burning of 1,2-dichloroethane, they discovered that the catalysts concerning catalytic oxidation was caused by their enhanced redox and acidic characteristics. Furthermore, for the catalytic breakdown of CVOCs, the catalytic performance of $MnO_x–CeO_2$ [25], CeO_2-CrO_x [26], and $Ru/Ti–CeO_2$ [28] also exhibited remarkable activity. It is anticipated that the doping of Ce in Cr_2O_3 will alter the materials relating absorption, photo-catalytic, and other physical and/or chemical characteristics. Consequently, it is now crucial to investigate Cr_2O_3 with Ce doping methodically. Furthermore, among them, non-metals have been employed; specifically, it is not given that the direct application of small molecular catalysts in environmental treatment will result in a decline in catalytic activity and a difficult recovery process. In order to address the aforementioned issues, it is customary practice to introduce a support, such as activated carbon (AC), carbon nanotubes, graphene, etc. Ning et al. designed a hybrid electro catalyst, $CuCo_2O_4/N-rGO$, which demonstrated that the introduction of graphene support could benefit the enhancement of electro catalytic activity and stability [29]. There exists however few published research on Ce-Cr_2O_3 support.

It was observed that among the many materials, activated carbon (AC) is widely used as supports or catalysts in the field of catalysis. Activated carbon (AC) has many surface functional groups and is inexpensive, making it a perfect carrier for transition metal oxides. Additionally, the porous structure of AC allows for improved dispersion and enhanced exposure of active sites on account to to its high surface area, unique surface chemical characteristics, superior stability, and biocompatibility [30]. Consequently,

we speculate that Ce-Cr_2O_3 can function better catalytically when AC is added. As previously indicated, AC can both increase Ce-Cr_2O_3 concerning ability to adsorb pollutants and give Ce-Cr_2O_3 a uniform dispersion that increases the number of active sites. Furthermore, AC might contribute by supplying electrons that hasten the production of reactive oxygen species (ROS) [31].

In summary, in order to catalytically oxidize CVOCs, this work methodically examines the implications of Ce on the catalytic activity of Cr_2O_3/Activated carbon catalyst, where DCE as the typical model reactant. The proportion of Ce/Cr and the preparation conditions were optimized. Different characetrization were the defining methods employed to assess the physicochemical properties of the xCe-Cr/AC catalysts in order to examine the impact of doping Ce on Cr_2O_3 supported activated carbon catalyst. Furthermore, its oxidation catalytic performance was assessed. With regard to better activity, selectivity, durability, and adaptability for DCE oxidation, we anticipate that this research will provide orientation for the creation and implementation of catalysts with exceptional effectiveness.

2. METHODOLOGY

2.1 Chemicals and Materials

Every reagent employed in the catalyst making procedure was of A.R. top-notch and was applied immediately. Shanghai Aladdin Biochemical Technology Co., Ltd. (Shanghai, China) supplied concentrated HNO_3 solution, cerium (III) nitrate nonahydrate (Ce $(NO_3)_3 \cdot 6H_2O$), chromium (III) nitrate hexahydrate (Cr $(NO_3)_3 \cdot 9H_2O$), pure terephthalic acid (PTA), and ammonium carbonate. whereas Pingdingshan Lvzhiyuan Activated Carbon Co., Ltd. supplied the activated carbon (AC).

2.2 Catalysts preparations

2.2.1 Preparation under hydrothermal method

The hydrothermal method was used to create the modified chromium-based catalysts. Firstly, activated carbon (AC) underwent a 400°C pre-treatment for 4 hours. Then, chromium nitrate Cr $(NO_3)_3 \cdot 9H_2O$, pre-treated AC, and purified terephthalic acid (PTA), nitric acid were mixed in 80 mL of de-ionized water until dissolved. Various amounts of cerium nitrate Ce

$(NO_3)_3 \cdot 6H_2O$ were added to form a homogenous solution. This was agitated for 2 hours, then heated at 210°C for 8 hours in an autoclave.

After filtering and rinsing, the precipitates were heated in ethanol at 100°C for 24 hours. The products were centrifuged, dried at 80°C, and calcined at 400°C for 4 hours. The dried solids were then ground and sieved to 40-60 mesh.

The catalysts were labeled xCe-Cr/AC, with x representing the proportional mass percentage of Ce (10-50%). A pure Cr_2O_3 catalyst was also synthesized similarly.

2.2.2 Preparation under co precipitation method

Pure CeO_2 was synthesized via co-precipitation. Ammonium carbonate was dissolved in 100ml of ultra-pure water. Concurrently, a predetermined quantity of cerium nitrate Ce $(NO_3)_3 \cdot 6H_2O$ was thoroughly dissolved in 100 mL of de-ionized water in separate beakers under conditions that facilitated stirring which was later added to the previous solution to form a homogeneous mixture. This was stirred at 80°C for 4 hours. The precipitate was filtered, washed to pH 7, and dried at 60°C overnight. The dried precursor was further dried at 100°C for 12 hours, then calcined at 400°C for 4 hours. Finally, the calcined material was sieved to 40-60 mesh to obtain the employed CeO_2 catalyst.

2.3 Catalysts Characterization

The synthesized catalysts were characterized by different tests and the details are described as follow,

Using the ASAP 2020 completely automatic surface area analyzer from McMurray Tec Instruments Co., Ltd., the textural features of the samples were extracted using nitrogen adsorption–desorption at −196 °C. The catalysts were degassed for three hours at 250 °C before to the measurement. The Brunauer–Emmett–Teller (BET) and Barrett–Joyner–Halenda (BJH) methods were used to calculate each catalyst's specific surface area (S_{BET}) and porous volume.

Using a 20 kV accelerating voltage, the Quant 250 FEG scanning electron microscope (SEM) was used to examine the sample's microscopic morphology, the Q150T gold spraying tool is used to spray gold over a sample's surface in order to increase the sample's conductivity and clarity of imaging. The energy dispersive spectra and element distribution on the sample's surface were observed using the energy dispersive spectroscopy (EDS, Oxford instrument).An X-ray diffractometer (XRD: model D8ADVANCE; Cu Ka radiation (40 kV, 40 mA, λ = 0.15418 nm)) was used to investigate the crystal phases of the materials, data were gathered at scattering angles (2h) with a step of 0.05° and a step speed of 0.1 s, spanning from 5° to 90°.

The catalysts relating surface elemental composition and elemental valence states were investigated, and both qualitative and quantitative analysis was carried out, using X-ray photoelectron spectroscopy (XPS, PHI QUANTERA II).

On a specially constructed TCD (thermal conductivity detector) setup, NH_3-TPD and H_2-TPR experiments were conducted utilizing 100 mg and 50 mg of catalysts, respectively. Catalysts were ground and sieved into a 40–60 mesh screen before the experiments to ensure a specific gas flow rate and an appropriate pressure drop. In order to conduct NH_3-TPD tests, catalysts were purged for approximately 3 to 4 hours with anhydrous NH_3 (4% in He) flowing at a rate of 33.3 ml/min. The catalysts were then heated in N_2 (33.3 ml/min) to achieve the desorption of NH_3. A temperature programmer was used to regulate the heating rate, which was 5 °C per minute, from 50°C to 900°C. In H_2-TPR tests, after pre-treatment trials with the feeding gas to completely eliminate contaminants such water on the catalysts surface, they were tested by raising the temperature from 50°C to 900°C at a linear heating rate of 5°C/min in pure N_2 containing 17% H_2 at a flow rate of 33,3 ml/min. In real time, the gas chromatograph observed and gathered data.

2.4 Catalytic Activity Evaluation

Under temperature control, the 1,2 dichloroethane (DCE) catalytic oxidation was assessed in a U-shaped quartz tube with an inner diameter of 4 mm. All of the catalyst quartz sands were sieved through a 40–60 mesh screen. For each test run, 0.1 g (or about 0.1 mL) of catalyst was added to the tube inside the reactor, and quartz wool was packed at both ends of the catalyst bed to keep the catalyst from being removed by the reaction's air flow. The gas hourly space velocity (GHSV) was set at 20,000 mL/(g·h) with the feed gas flow rate regulated at 33.3 mL/min. A furnace with a preset temperature regulates the temperature of the

fixed bed reactor. The temperature was gradually increased from 200 °C to 380 °C (heating at a rate of 5 °C/min), and a gas chromatograph fitted with a TCD and FID for the quantitative analysis of organic compounds, CO_2 and CO, was used to examine the effluent gas. Following five minutes of maintenance at each test temperature, conversion measurements and product profiles were obtained. The conversion data consisted of the average of three sampling studies. The conversion of DCE was computed using the following formula,

$$X_{1,2-DCE} = \frac{C_{in} - C_{out}}{C_{out}} \times 100\%$$

Eq. 1. Conversion rate

Where,

$X_{1,2-DCE}$, is the conversion rate of DCE,
C_{in} and C_{out}, represent the inlet and outlet concentrations (ppm) of DCE.

When the reaction efficiency of DCE is below 20%, the reaction rate would be described as an alternative formula, as follows:

$$r = -kc = [-A exp(-E_a/RT)]c$$

Eq. 2. Reaction rate

Where,

A, is the pre-exponential factor,
T, the test temperature (K),
R, denotes the ideal gas constant $(J.mol^{-1}.K^{-1})$,

Ea is the apparent activation energy $(J.mol^{-1})$.

For DCE conversion efficiencies less than 20%, activation energies were computed at low temperatures using Eq. 2 simplified into Eq. 3,

$$Ln\ r = \frac{-Ea}{RT} + C$$

Eq. 3. Arrhenius theory

The following equation was used to determine the turnover frequency,

$$TOF\ (S^{-1}) = \frac{XC_0}{n_M}$$

Eq. 4. Turnover frequency

Where,

X, represents the DCE conversion efficiencies of different catalysts at certain temperatures,

C_{DCE} (Or C_0), the feed concentration of DCE $(mol.L^{-1})$,

n_M, the molecular amount (mol) of the catalyst.

3. RESULTS AND DISCUSSION

3.1 N₂-BET Analysis

Fig. 1(a, b) displays the N_2 adsorption-desorption isotherms, the Barrett-Joyner-Halenda (BJH) pore diameter distribution of pure Cr, and the modified catalysts. According to IUPAC categorization [32], each sample exhibited a unique type IV adsorption/desorption isotherm with H_3-type hysteresis loops, as shown in Fig. 1(a). This implied that a mesoporous structure was present. As shown in Fig. 1(a), the addition of Ce and activated carbon improved the characteristics of the Cr_2O_3 catalyst much more. There are even more mesopores in the samples, as seen in the modified Cr's hysteresis loop dropping to even lower levels at roughly 0.4.

As noticed in Fig. 1(b), every catalysts are mostly found as mesopores, with the majority of these pores being concentrated between 2 and 35 nm. This suggests that the catalysts' pore size distribution is homogenous. These findings establish that the bulk structure's breakdown and the creation of a stable composite metal oxide catalyst are both aided by the preparation technique and the four hours of calcination at 400°C.

Table 1 provides an overview of S_{BET}, mesoporous surface area (Ames), and pore volume (Vp). In every sample, pure mesoporous structure is present. With 20CeCr/AC, having largest S_{BET} (234.42 m²/g) values. Additionally, of the modified Cr with various Ce molar doping ratios, 20Ce-Cr/AC has the greatest Vp (0.5165 cm³ /g). Higher S_{BET} and pore volume were said to maximize the ability of VOCs to adsorb and reduce transfer resistance [33].

Table 1 demonstrates the significant impact that varying Ce doping percentages have on the catalyst structure. The catalysts concerning S_{BET} and Vp increase first, then drop, upon doping Ce into the Cr. As the concentration of Ce rises, excess Ce will cover the active sites on Cr_2O_3,

suggesting that the excess doped Ce was not only deposited on the surface of AC but also filled its pores, resulting in a reduction of catalytic activity. Consequently, the amount of doped Ce directly optimized the catalysts surface and structural characteristics, which evidently have a major effect on the catalysts performance.

3.2 XRD Analysis

The XRD patterning of the modified accompanied by the pure catalysts are displayed in Fig. 2, and Table 1 contains the relevant data. All catalysts have XRD peaks that are found to be expressed in the 5–90° range. As can be seen from Fig. 2(a), for the CeO_2 sample, all four of the detected diffraction peaks could be correctly ascribed to the fluorite structure of CeO_2. The average crystallite sizes of all the samples were determined using the Scherrer Formula, CeO_2 crystallite size was calculated to be around 10.64 nm. On the other hand, the Cr_2O_3 showed a more pronounced XRD pattern, which are attributed to the hexagonal phase of Cr_2O_3. The later has more well-defined crystal planes, as shown by the presence of more diffraction peaks. Additionally, the XRD study showed that Cr_2O_3 had an average crystallite

size of roughly 20.56 nm, which was bigger. The size of each solitary crystalline domain within a material is referred to as the crystallite size. The size of the coherent scattering regions within the material increases with crystallite size. This finding implies that the Cr_2O_3 sample's bigger crystallites grew more quickly. This line on the fact that Cr_2O_3 is a better base catalyst.

Fig. 2(b) showed that the spinel structure of Cr_2O_3 was preserved upon the addition of Ce; nevertheless, a new diffraction peak at 26.59 ° was identified as the cubic CeO_2 diffraction peak, and no additional discernible diffraction peaks of the fluorite-structure of CeO_2 species were found. To add, the major diffraction peaks of the hexagonal phase Cr_2O_3 were somewhat moved to an elevated angle side (Fig. 2(b)). This was because Ce ions were once again incorporated within chromium lattice, leading to the inception of Ce-Cr solid solution, that improved the ability for storing and releasing oxygen. The modified catalyst's diffraction peaks are not as strong as those of the pure Cr; where Cr_2O_3's average crystallite size, which was approximately 20.56 nm, decreases in tandem with the addition of Ce. The dimensions and crystallinity of the sample frequently correlate
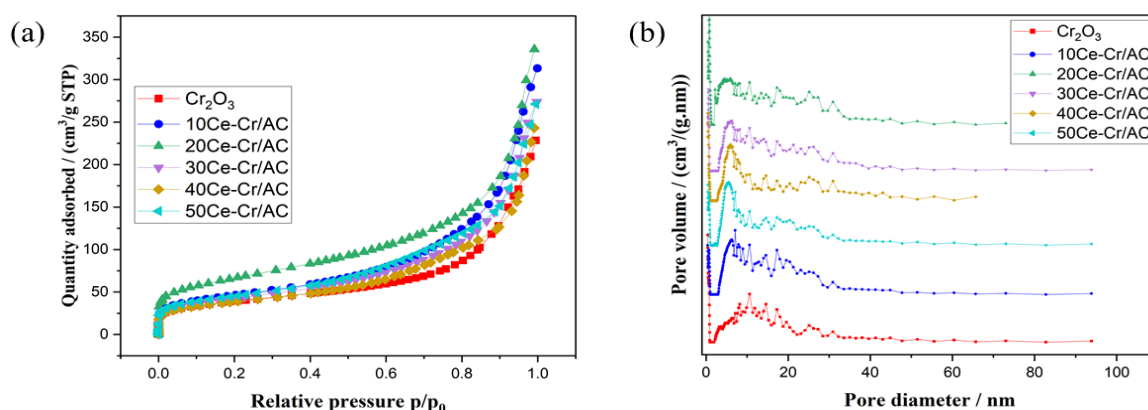

Fig. 1. N₂ adsorption/desorption isotherms (a) and pore size distribution (b) of the samples

Table 1. Profiles data of the catalysts

Samples	S_{BET} [a] (m² /g)	A_{mes} [b] (m² /g)	V_P [c] (cm³ /g)	Pore diameter(nm)	Cristallite size (nm)
Cr_2O_3	139.34	155.38	0.3429	9.8334	20.56
10CeCr/AC	163.47	187.24	0.4666	11.418	18.22
20CeCr/AC	234.42	268.52	0.5165	8.8125	13.09
30CeCr/AC	150.99	168.77	0.4115	10.902	15.29
40CeCr/AC	137.89	148.07	0.3743	10.859	15.61
50CeCr/AC	158.66	183.3	0.4058	10.23	14.19

[a] Surface area, [b] Calculated using BJH method, [c] Total pore volume estimated at p/p₀=0.99.
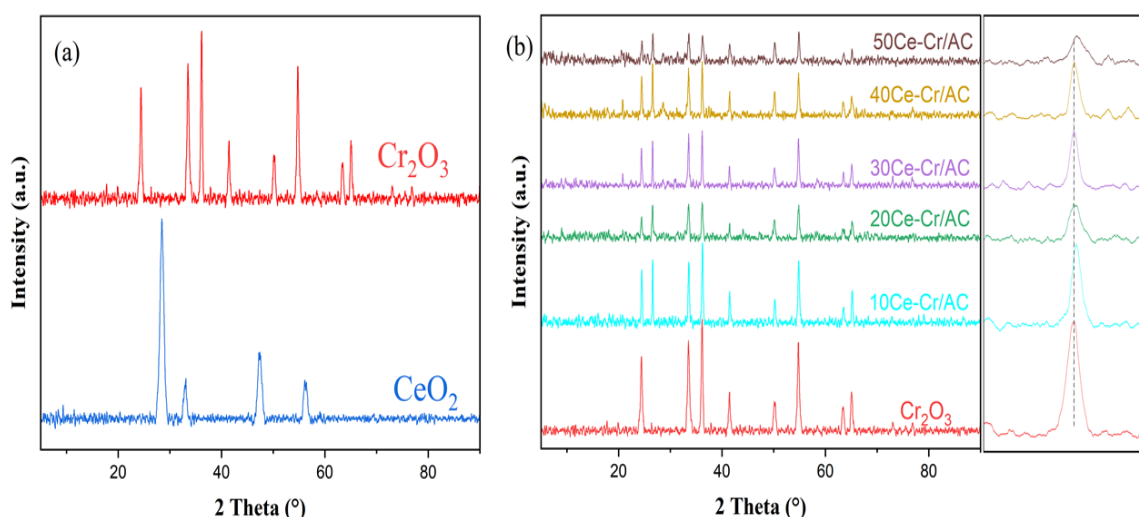
Fig. 2. XRD patterns of the pure (a) and modified (b) catalysts

with the width and intensity of diffraction peaks. Furthermore, as the diffraction peak width increases, the crystal size decreases [34]. Among catalysts, the diffraction peaks of 20Ce-Cr/AC are broader and less intense. This implies that even while the crystallinity of 20Ce-Cr/AC is lower, its crystal size is smaller, which may result in more active sites for the catalytic activity. 20Ce-Cr/AC has therefore better catalytic performance for DCE combustion.

3.3 SEM and EDS Analysis

SEM pictures were utilized to visually inspect the various microstructures proper to the catalysts. It is evident from Fig. 3(a, b) that the morphology of the Cr_2O_3 catalysts expressed in a typical polyhedral shape. More active sites are exposed by the Cr structure, which is advantageous for the combustion of CVOCs.

Following the addition of Ce (Fig. 3(d-h)), the xCe-Cr/AC products can largely retain their amorphous shape. As seen in Fig. 3(e), the particles of 20Ce-Cr/AC are tiny and evenly distributed among them. In addition to ensuring that the grain surface is utilized to its fullest potential during the catalytic process, More active sites may be exposed to CVOC molecules as a result of the integration structure formed by CeO_2 nanocrystallites at 20Ce-Cr/AC, which is beneficial for the adsorption of CVOCs.Put otherwise, there is a chance that this structure will quicken the reaction's kinetics. As seen in Fig. 3(d-h), in comparison to 20Ce-Cr/AC, the remaining catalyst exposed bigger and aggregated particles, which will not be favorable for the exposure of active sites.

EDS analysis of 20Ce-Cr/AC was carried out to validate the formation of xCe-Cr/AC composite. Different locations were focused during the test, and Fig. 4 displays the related EDS-mapping diagrams. The catalyst surface only contains the components Ce, Cr, C, and O; in which all components are uniformly dispersed throughout the catalyst surface. The Ce/Cr atomic ratio is nearly in line with the theoretical doped percentage, indicating that the Cr-supported AC catalyst surface has received the necessary percentage of Ce doping to create 20Ce-Cr/AC. Table 2 contains specifics of the EDS spectra of the electrospun 20Ce-Cr/AC values expressed in weight percentage.

Table 2. Element contents of 20Ce-Cr/AC

Elements	Mass fraction(wt%)
C	19.11
O	25.39
Cr	32.82
Ce	22.69
Total quantity	100

3.4 XPS Analysis

Using the XPS spectra of Cr 2p, Ce 3d, and O 1s, Fig. 5 illustrates the surface oxidation states of Cr_2O_3 , CeO_2, and 20Ce-Cr/AC catalysts studied. Fig. 5(a) displays the catalyst's Cr 2p XPS spectrum. The $2p_{1/2}$ bond energies of Cr^{3+} and Cr^{6+} are placed at approximately 584.1 eV,

while the $2p_{3/2}$ bond energies of Cr^{3+} and Cr^{6+} are positioned at approximately 574.5 eV, respectively. These values show that the Cr element coexists with Cr^{3+} and Cr^{6+} on the catalyst's surface. Deep oxidation of DCE can be aided by Cr^{6+}'s significant oxidation capacity. The Ce 3d XPS spectra for each sample appears in Fig. 5(b), revealing multiple peaks at 880.6 eV, 883.5 eV, 886.3 eV, 896.5 eV, 898.7 eV, 905.1 eV, and 914.9 eV; these peaks are tagged to Ce $3d_{3/2}$ and Ce $3d_{5/2}$, accordingly. The fact that bond energies attributed to Ce^{3+} and Ce^{4+} are allocated to each peak confirms the coexistence of Ce^{3+} and Ce^{4+} in the samples. Ce^{3+}/Ce^{4+} ratios for the samples are computed using integrated areas of XPS peaks (as illustrated in Table 3), and it was clear that the sample with the highest relative concentration of Ce^{3+} ions was the 20Ce-Cr/AC catalyst. Higher Ce^{3+} concentrations were found to encourage the development of charge imbalances, oxygen vacancies, and unsaturated chemical bonds on catalyst surfaces, which may enhance DCE's catalytic oxidation capabilities [35,36]. Furthermore, increased Ce^{3+}

concentrations enhance the mobility of the active oxygen species, potentially improving catalytic performance for the oxidation of volatile organic compounds. As a result, the 20Ce-Cr/AC catalyst would demonstrate outstanding catalytic performance.

The samples' O1s XPS spectra are displayed in Fig. 5(c), where they are separated into two peaks at binding energies between 525.70 eV and 533.3 eV. This is attributed to lattice oxygen (O_{Latt}), which is mostly derived from AC, Cr, and the doped Ce; on the other hand, adsorption oxygen (O_{Ads}) is primarily caused by the presence of surface-adsorbed oxygen, which are hydroxyl OH^-, carbonate $CO3^{2+}$, and $O2^{2-}$ or O^-. The catalyst surface's O_{Latt}/O_{Ads} ratio sequence is as follows: 20Ce-Cr/AC > Cr_2O_3 > CeO_2. This suggests that 20Ce-Cr/AC possesses the majority of the O_{Latt} species, the removal of which may lead to the creation of oxygen vacancies. As a consequence, it is verified that the 20Ce-Cr/AC has the greater number of oxygen vacancies, and the findings agree with Ce 3d XPS.
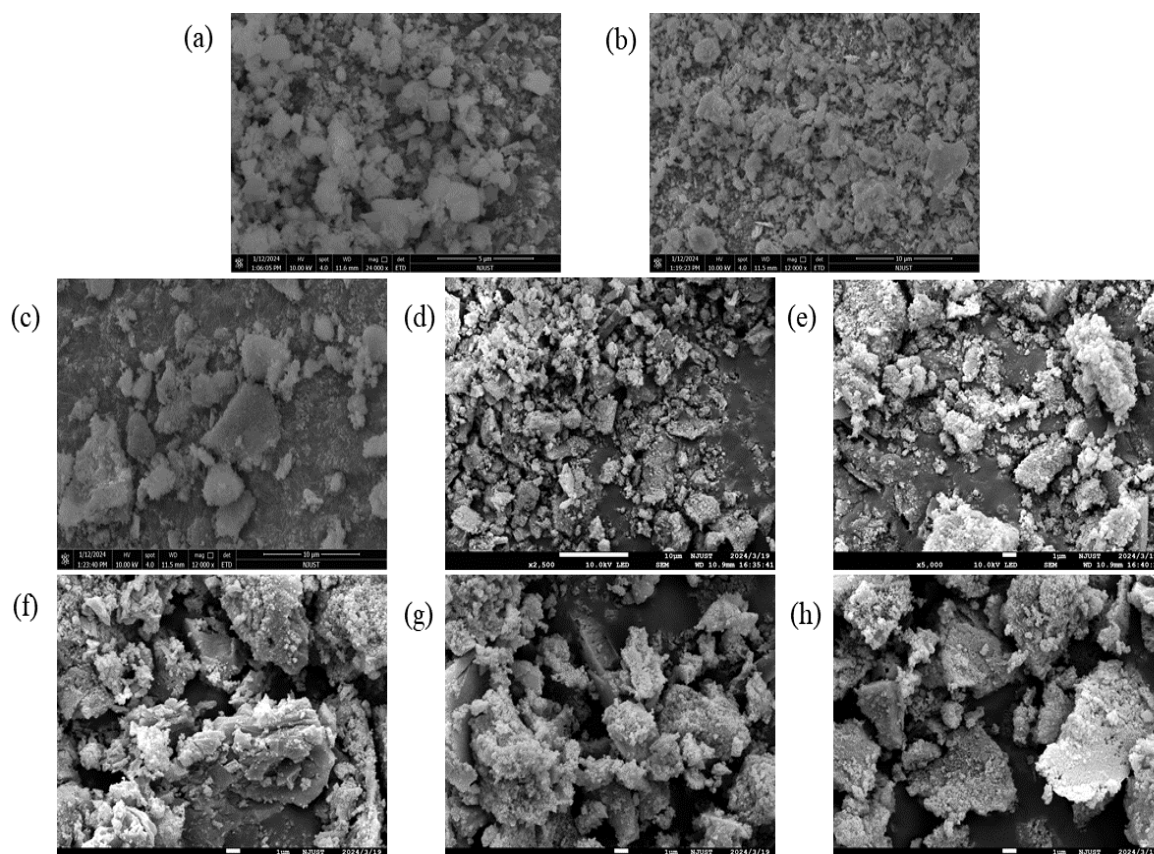

Fig. 3. SEM images of Cr_2O_3 (a), CeO_2 (b), activated carbon (c), 10Ce-Cr/AC (d), 20Ce-Cr/AC(e), 30Ce-Cr/AC(f), 40Ce-Cr/AC(g), 50Ce-Cr/AC (h)
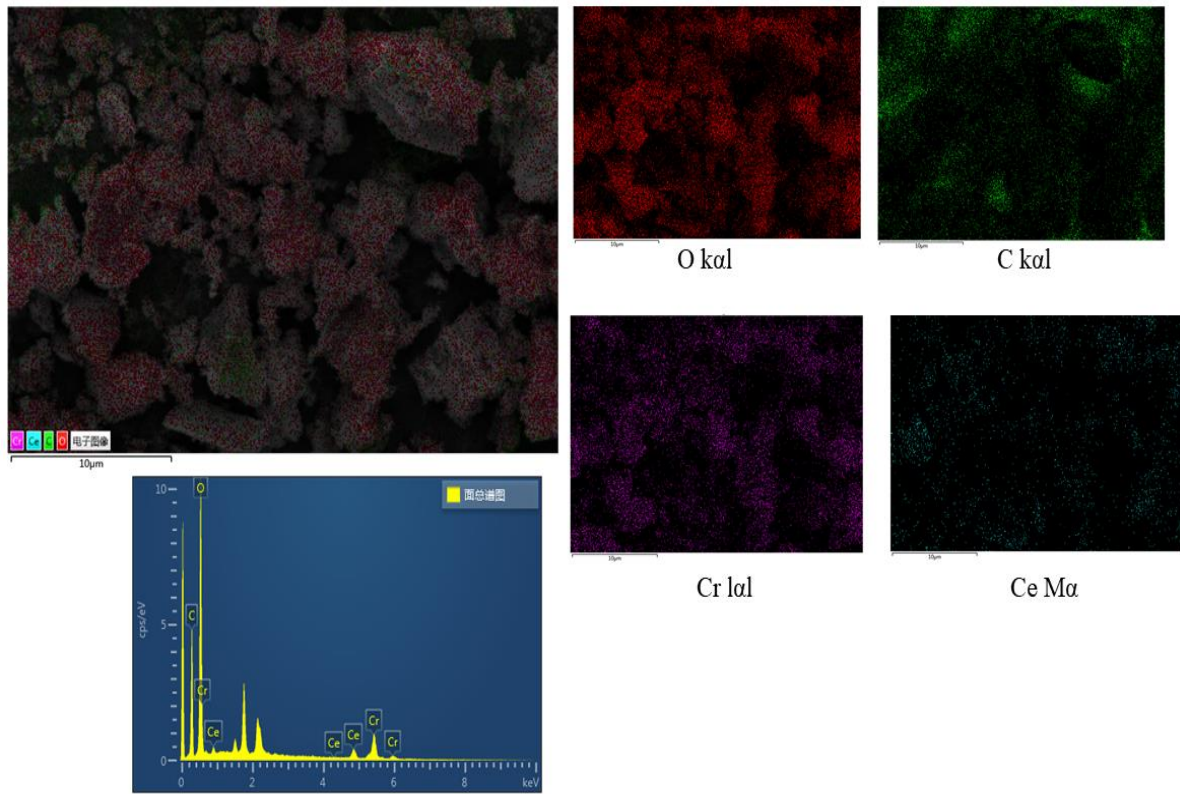
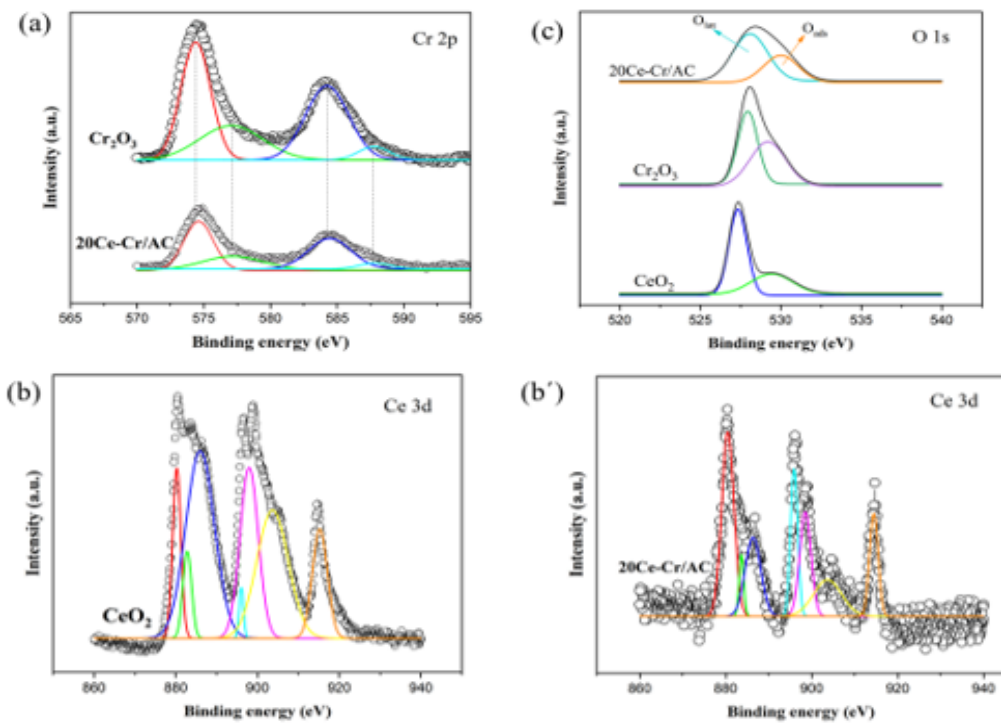**Fig. 4. Elemental mapping images and EDS spectrum of the 20Ce-Cr/AC catalyst**

Fig. 5. The XPS spectra of Cr_2O_3, CeO_2 and 20Ce-Cr/AC catalysts. (a) Cr 2p; (b) Ce 3d and (c) O 1s

The results stated above indicate that CeO_2 and Cr_2O_3 can interact to boost the amount of Ce^{3+}, Cr^{6+}, and OLatt on the catalyst surface, leading to better catalytic performance for DCE catalytic oxidation. It is anticipated that level up surface oxygen vacancies of 20Ce-Cr/AC will aid in improving DCE and oxygen molecule adsorption.

3.5 H$_2$-TPR Analysis

The redox characteristics is one of the most significant aspects of catalysts for CVOCs oxidation processes. The H_2-TPR profile of pristines is displayed in Fig. 6(a). Within the test temperature range, only one reduction peak is detected for CeO_2 at around ~100℃ and some low intensity reduction peak at ~100℃ and 500 ℃ for AC. The decrease in both surface and subsurface oxygen levels accounted to these peaks; the absence of any other peaks indicates their low reducibility. In contrast, the Cr_2O_3 catalyst profile shows an initial peak reduction begining at lower temperatures (80°C), and that this increased lattice oxygen diffusion in the superficial layer led to the appearance of more new peaks with stronger intensities, indicating a notable improvement in reducibility. These findings demonstrate once more how important, the chosen base catalyst is to the final product's characteristics, where Cr_2O_3 excelled in this instance.

The H_2-TPR profiles all modified Cr-based catalysts are shown in Fig. 6(b). Overall, for every sample, the reduction below 900 °C could be separated into two distinct stages: a low-temperature reduction (LTR) at 400 °C or less, which is most engaging from a catalytic perspective because it is most likely linked to redox active sites on the catalyst surface, and a high-temperature reduction (HTR) at higher temperatures, which is primarily linked to bulk and sub-surface reduction processes. The precise temperature range of reduction varies depending on the sample. When compared to Cr_2O_3, the newly developed catalyst's TPR profiles were unique. In specifics, the peaks at LTR mostly correspond to H_2 consumption by bulk lattice oxygen ($O_{Latt'}$), chemically adsorbed oxygen (O_{Ads}), and surficial lattice oxygen (O_{Latt}). It's interesting to note that, the modified catalysts peak intensity and range were increased. This was ascribed to the increased lattice oxygen mobility brought on by the formation of vacancies or structural defects, which further promoted the redox property and ultimately improved catalytic performance. The findings showed that adding

Ce to Cr_2O_3 may increase the catalyst reducibility. Additionally, the interaction of CeO_2 and Cr_2O_3 increases the fluidity of reactive oxygen species on the catalyst surface. Using activated carbon as a support may also contribute to the abundance of reducible oxygen species by increasing the number of active sites available.

The bulk reduction of the Cr_2O_3 particle was attributed to the peak at HTR. Due to the strong interaction between CeO_2 and CrOx, particularly for the 20Ce-Cr/AC catalyst, there is an apparent increase in the amount of Cr^{6+} species when compared to pure Cr_2O_3. This peak intensity is attributed to the reduction of Cr^{6+} to Cr^{3+}. Since Cr^{6+} requires more coordinated oxygen atoms than Cr^{3+}, more oxygen vacancies may occur as a result of the creation of additional Cr^{6+} species. However, the changed catalysts HTR peaks have mostly moved to higher temperatures. This change may be attributed to the creation of more stable Ce-Cr_2O_3 or the inhibiting influence of non-reducible Ce atom species occupying the active site in the spinel structure of Cr_2O_3, which made Cr^{6+} less reducible.

Furthermore, as cerium concentrations rise, the intensity of H_2 consumption first increases and then gradually decreases. The majority of Cr^{6+} ions are found as bulk Cr_2O_3 or tiny clusters, which can be covered with CeO_2 throughout the reduction-oxidation processes. It is challenging to reduce the scattered Cr_2O_3 and CeO_2 because of the kinetic diffusion. Furthermore, not all of the Cr^{6+} in Ce-Cr solid solutions is eliminated entirely. Therefore, it makes sense that as the concentration of cerium species rises, H_2 consumption will decrease. In Ce molar percentage ratios of xCe-Cr/AC, the reduction peak intensity sequence follow 20 < 10 < 30 < 50 < 40. The sequence is consistent with the catalytic activity for DCE combustion, the catalytic activity increases with decreasing reduction peak temperature. This demonstrates once more how important the proper amount of doping is during synthesis. Furthermore, in accordance with its ideal catalytic activity, 20Ce-Cr/AC has the biggest hydrogen consumption reduction peak area, indicating that it has the largest amount of reactive oxygen species.

3.6 NH$_3$-TPD Analysis

NH$_3$-TPD was employed to assess the surface acidity of the pure and modified catalysts, as Fig. 7 illustrates. The acid sites on the catalyst
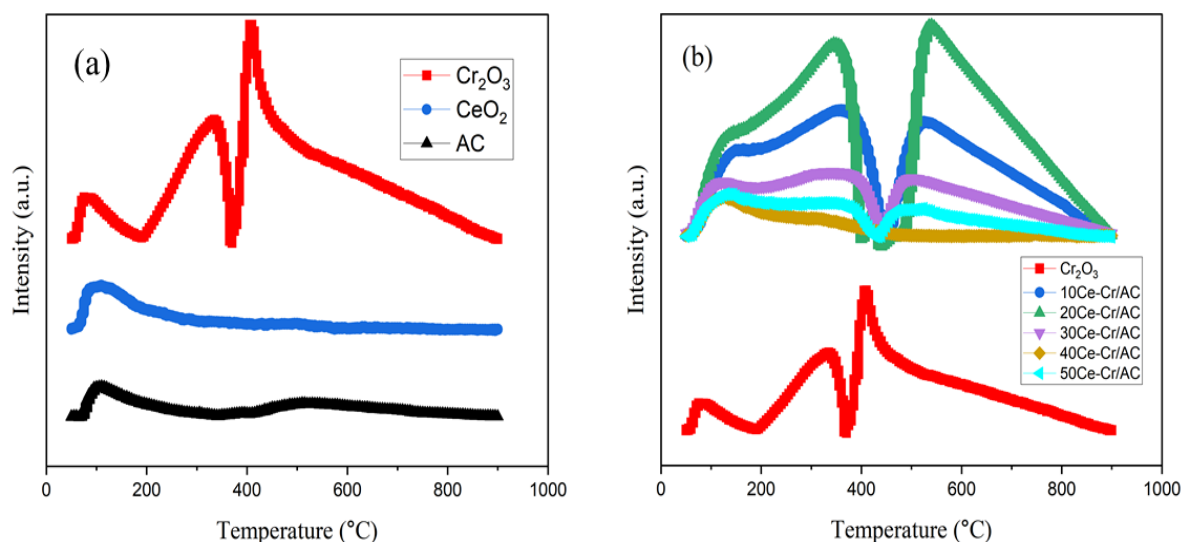
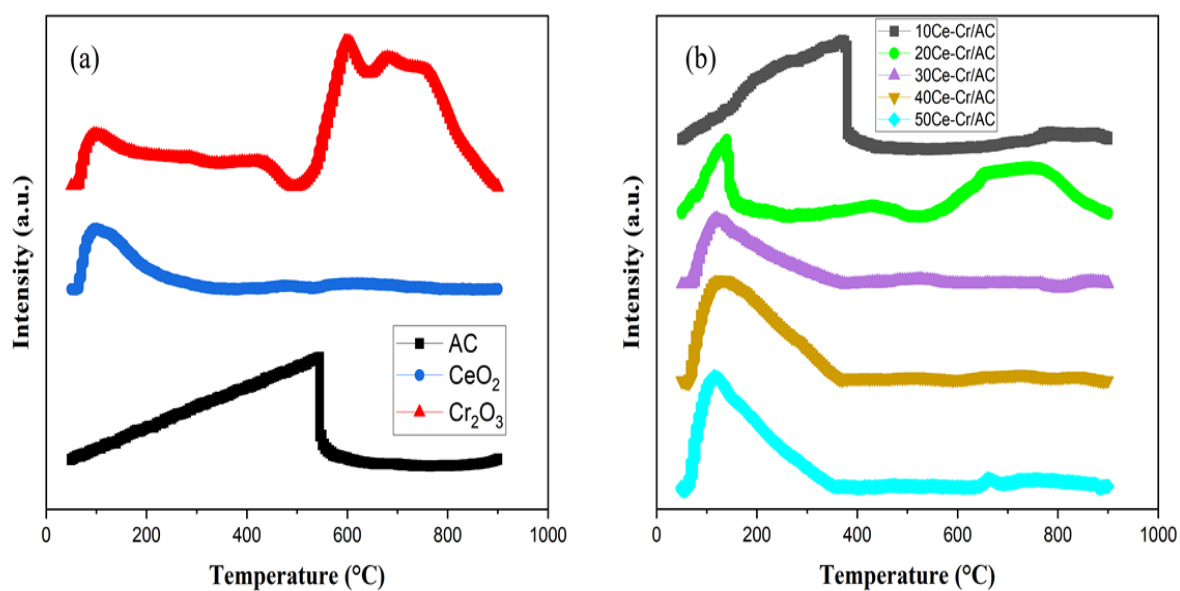**Fig. 6. H₂-TPR of the pure (a) and modified catalysts (b)**

Fig. 7. NH₃-TPD of the pure (a) and modified catalysts (b)

surface can effectively stimulate the breakage of C-Cl bonds during the catalyst catalytic degradation of CVOCs reaction process, hence increasing the catalytic activity.

The pure catalyst displayed many peaks, as depicted in Fig. 7(a). The desorption peaks at approximately <300℃, 300℃-600∘C, and 600℃> were ascribed to weak, medium, and strong acid sites, respectively. The peak regions were utilized to quantitatively compare the variations in

acidity. It was evident that weak and medium acid sites predominated in both AC and corresponding CeO_2 catalysts. This was particularly true for AC, which has a broad NH_3 desorption peak that spans the temperature array of 55°C to 545°C and covers weak acid and medium strong acid acid sites. Consequently, a lot of acidic sites can be provided by utilizing activated carbon as a catalyst support, which enhances catalytic activity. In contrast Cr_2O_3 displayed many desorption peaks, one of which was associated

157

with strong acid sites and had a high desorption intensity at around 600°C. This demonstrates once more it as ideal base.

The NH_3-TPD profile of the modified catalysts is displayed in Fig. 7(b). As can be seen, the catalyst originally followed the profile of activated carbon. However, the coverage range was determined to be between 60 and 400°C at 10% loading, and as the Ce loading grows, the region of the NH_3 desorption peak gradually diminishes. This is because part of the activated carbon acidic sites are covered by the loaded Ce; lowering the exposure causes the acidity to lessen. The catalyst begins to adopt the pure Ce profile found at the weak acid point as the loading percentages increases. On the NH_3-TPD spectrum of the 20Ce-Cr/AC catalyst, a new, weakly intense desorption peak arises at about 600°C. This peak is the same as the potent acid peak that was previously observed on the pure

Cr. The peak intensity fully decreases as the load increases. This demonstrates that an appropriate doping concentration of Ce on the Cr/AC surface will result in an interaction that modifies the acid site, which is in line with the findings of the XRD (see to section 3.2).

Nonetheless, the xCe-Cr/AC catalysts have lower As (strong acid) values, suggesting that the inclusion of CeOx clearly reduces strong acidity. Both strong and weak acid sites are crucial for the oxidative degradation of CVOCs [37]. It is evident that 20Ce-Cr/AC has substantially higher catalytic activities than other catalysts for the destruction of CVOCs. It suggests that the right strength and density ratio of strong to weak acidity is beneficial to the development of CVOC catalytic degradation ability, and that the combination of Cr_2O_3–CeO_2 and activated carbon enhances the dehydrochlorination of volatile organic compounds (VOCs).
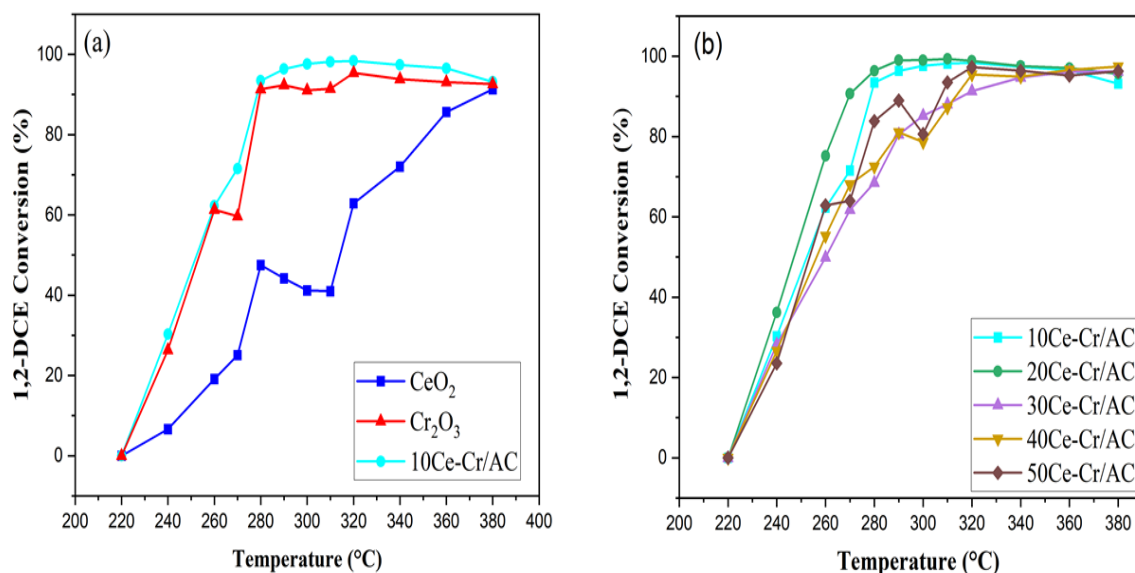

Fig. 8. The catalytic performance of different prepared catalysts for 1,2-Dichloroethane combustion

Table 3. Catalytic activities, activation energies (Ea) and element state of the prepared catalysts

Catalysts	$T_{50\%}$ (°C)	$T_{90\%}$ (°C)	Ea (kj/mol)	Cr^{6+}/Cr^{3+}	Ce^{3+}/Ce^{4+}	O_{latt}/O_{ads}
CeO_2	314	375	135.191	-	0.42	3.21
Cr_2O_3	253.5	279.6	288.242	0.68	-	4.22
10Ce-Cr/AC	252	278	390	-	-	-
20Ce-Cr/AC	247	269.5	392.985	0.74	0.57	5.88
30Ce-Cr/AC	260	316	308.232	-	-	-
40Ce-Cr/AC	256	313.3	291.474	-	-	-
50Ce-Cr/AC	253	307.2	258.770	-	-	-

3.7 Catalytic Oxidation Performance Test

Fig. 8 reveals the profile temperature dependency of catalytic efficiency for DCE conversion over catalysts under the following conditions; clean air was used as the reaction gas and input gas, DCE concentration was set at 1000 ppm and SV was set at 20,000 mL/(g h). Fig. 8(a) displays the catalytic efficiency of the pure catalysts and the 10Ce-Cr/AC catalyst. When it comes to DCE oxidation, "Cr_2O_3" has significantly greater catalytic activity than others when used alone, whereas "CeO_2" exhibits the lowest. It should be highlighted that while the Cr_2O_3 and The modified Cr low-temperature activities are quite near to one another, there is a noticeable increase in the distance between the catalytic activities as the temperature rises. The thermal sintering mechanism may be able to explain the phenomenon of different catalytic activity across temperature zones [38,39]. The primary transfer pathways for O_{Sur} (O^-, O^{2-}), which are mostly in charge of the catalytic activity at low temperatures, are provided by lattice defects and oxygen vacancies in the non-stoichiometric Cr_2O_3. As the reaction temperature rises, Cr_2O_3's physico-chemical properties change. The solid-phase structure is rearranged, lattice flaws and vacancies are reduced, the valence of Cr ions is altered, and other modifications take place. Moreover, the migration and valence shift of metal ions are facilitated by the lattice defect and oxygen vacancy transfer pathways. Consequently, the accumulation of these effects usually results in a decrease in activity. As a result, the modified catalysts created from Cr_2O_3 in this work exhibits both great catalytic activity and superior high temperature stability.

Even though Cr_2O_3 performed well, all of the single metal-based catalysts showed multiple deactivations at various high temperatures during the performance, which is related to poisoning impacts. In comparison to pure CeO_2 and Cr_2O_3, the modified Cr based catalyst performed significantly better. According to these outcomes, CeO_2 and Cr_2O_3 exchanges plus the use of activated carbon as a support can enhance the catalytic activity for DCE oxidation. As mentioned before, AC can boost the adsorption capacity of $xCe-Cr_2O_3$ for pollutants and give a uniform dispersion of $xCe-Cr_2O_3$ to provide more active sites. Moreover, AC may be involved by granting electrons that quicken the generation of ROS. Which in our instance has been shown its effectiveness; the catalyst has stabilized and the

deactivation appears to be disappearing. The following is the order of catalytic activity: 10Ce-Cr/AC > Cr_2O_3 > CeO_2. The modified catalyst has the highest activity of all of them, and it can fully degrade DCE at lower temperatures.

The amount of Ce doped in the Cr/AC based catalyst had a significant impact on its performance, as seen in Fig. 8(b). Their performance appear to correlate with the percentage doped rises, resulting in an increase in catalytic activity. However, the performance of the modified catalyst decreased concurrently at a percentage of ≥30 doped Ce. The active sites on Cr_2O_3 will be covered by the excess Ce concentration, which has an impact on the S_{BET} and V_P of the catalysts as indicated in Table 3. This will result in a decrease in catalytic activity. Therefore, the catalytic activity of $xCe-Cr/AC$ is significantly influenced by the proper preparation technique as well as the proportion of Ce that is doped. As can be seen in Table 3, 20Ce-Cr/AC performed the best out of all the catalysts, with T_{50} at 247°C and T_{90} at 269.5°C. The following is the sequence in which the catalysts function during DCE combustion: 20Ce-Cr/AC > 10Ce-Cr/AC > Cr_2O_3 > 50Ce-Cr/AC > 40Ce-Cr/AC > CeO_2.

In order to study the reaction of 1, 2-DCE on the series of catalysts, kinetic calculations were performed on them. As illustrated in Eq. 2, the catalytic combustion of 1, 2-DCE under excess oxygen adheres with the first order kinetics mechanism tied to DCE concentration, according to literature reports [40].

Therefore, the key to determining the value in Eq. 3, which is used to the derivation of activation energy (Ea) at lessen conversion (a mere 20%), was to use the Arrhenius plots in Fig. 9. Based on that, Arrhenius plots is presented in Fig. 9 and the Ea values among the catalyst is illustrated in Table 3.

Apparent activation energies (Ea) were calculated with 95% confidence limits based on the relation of rate to temperature below 20% conversion. Looking at the profiles of the pure catalyst, Cr_2O_3 exposed the highest Ea at 288.242 Kj/mol which coorelate with he temperature controlled conversion program. In Fig. 9(b), a significant increase in Ea over the modified catalysts is observed, especially for 20Ce-Cr/AC (392.985Kj/mol). Here, the increase in Ea is due to crucial Cl adsorption. Which can be concluded to a stronger conversion of DCE.

The different Ea values during the reaction can be ascribed to the difference both in H_2O and Cl concentration of products and in surface oxygen needed for different CVOCs oxidation.
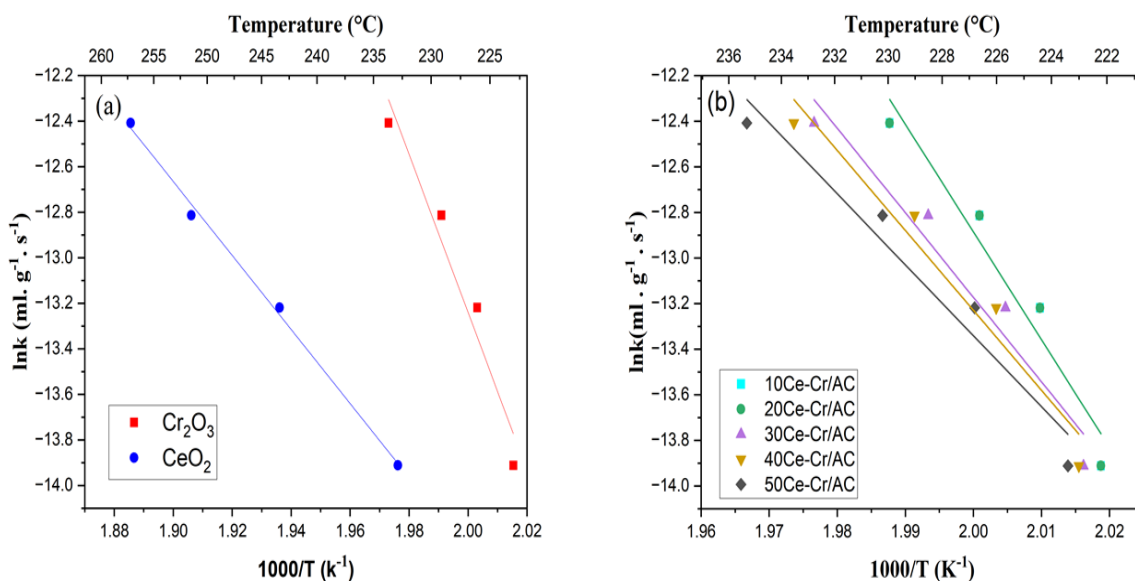

Fig. 9. Arrhenius plots of the pure (a) and modified catalysts (b)
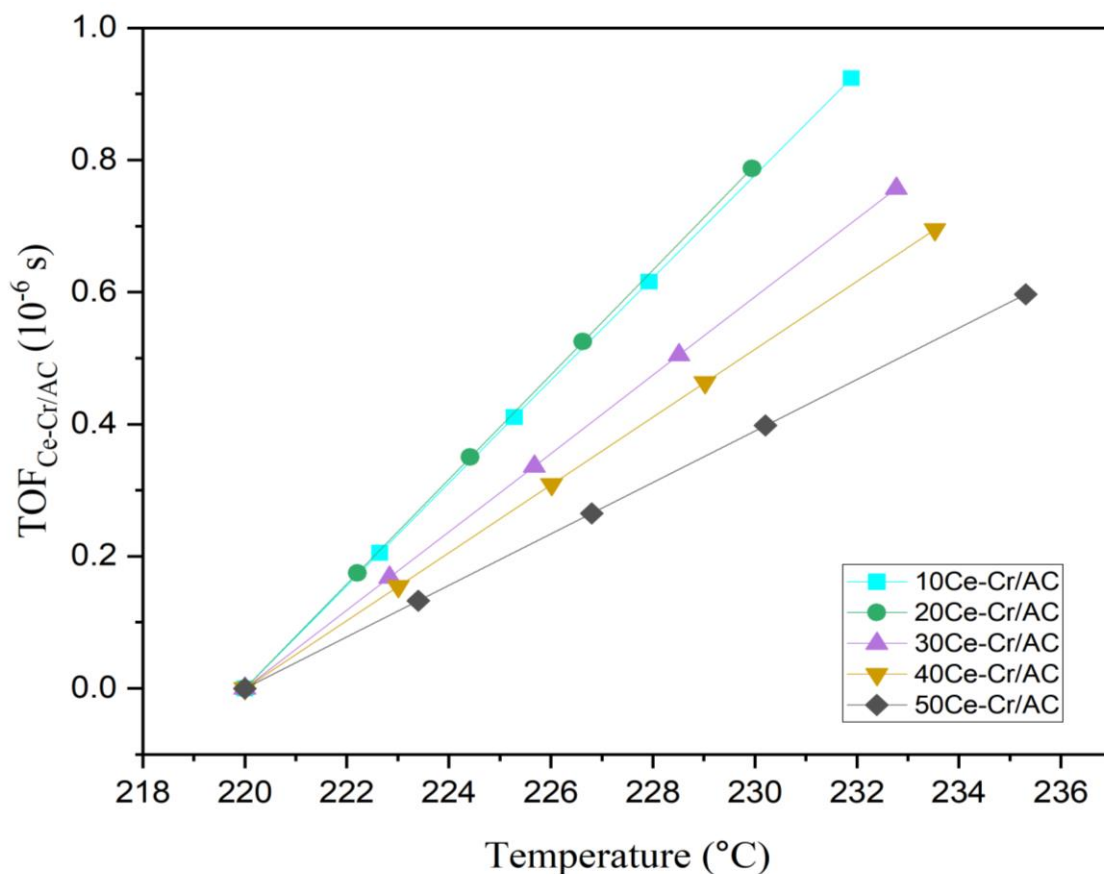

Fig. 10. Turnover frequency (TOF) of the modified Cr based catalysts

Plots of turnover frequency (TOF) values for lower DCE conversion (a mere 20%) are shown in Fig. 10 as reaction temperature increases, where the Eq. 4 was employed.

With the increase in Ce species on Cr/AC particles, TOF decreases slowly, and 50Ce-Cr/AC showed the lowest TOF of 0.1 – 0.5 (10^{-6}s). The oxidation of alkoxy and enolic compounds as well as their synthesis should benefit from the increase in Ce species. Strong Cl adsorption on Lewis-acidic Ce ions is responsible for a significant drop in TOF over. Therefore, regardless of the composition of CVOCs, TOF is dependent on Cl removal. This phenomen has been prooved during the catalytic performance of pure CeO_2 over 1,2-DCE showed in Fig. 8, the convertion profile of the pure CeO_2 expressed a low catalytic activity accompanied by several deactivation during the performance. The TOF parameters of the catalysts ascend in the sequence of 50Ce-Cr/AC < 40Ce-Cr/AC < 30Ce-Cr/AC < 10Ce-Cr/AC < 20Ce-Cr/AC, which confirm that 20Ce-Cr/AC has the most prominant catalytic efficiency.

4. CONCLUSION

For the deep catalytic oxidation of DCE, a series of highly active xCe-Cr/AC catalysts were produced. Following the characterisation methods mentioned, the study shows how crucial the cerium (Ce) doping level and catalyst synthesizing technique are in adjusting the physicochemical characteristics and catalytic efficiency of chromium-based catalysts for the molecule reduction of 1,2-dichloroethane. It was discovered that the Cr-based catalysts acidity, reducibility, and textural qualities were all enhanced by the introduction of Ce and activated carbon. The maximum catalytic activity was found in the 20Ce-Cr/AC catalyst, which was explained by its ideal Ce doping level, which improved the redox characteristics and revealed more stable structure and active sites by exposing the largest S_{BET} and Vp. The largest concentration of Ce^{3+} ions and lattice oxygen species were found in the 20Ce-Cr/AC catalyst, according to the characterization data. This enhanced the catalytic oxidation performance by easing the adsorption and activation of DCE and oxygen molecules.

Subsequent investigations may examine the enduring stability and regeneration of the 20Ce-Cr/AC catalyst in order to evaluate its pragmatic suitability for mitigating volatile organic molecules.

Further research might be done on the catalytic mechanism and the support material's function in improving the redox characteristics and oxygen mobility. It would be beneficial to broaden the research to include additional kinds of volatile organic molecules in order to gain greater insights of the catalysts relating adaptability.

COMPETING INTERESTS

Authors have declared that no competing interests exist.

REFERENCES

1. Chunhao DAI, Yaoyu Zhou, Peng Hui, Shaojian Huang, Pufeng Qin et al. Current progress in remediation of chlorinated volatile organic compounds: A review. Journal of Industrial and Engineering Chemistry. 2018;62:106-119.
2. Haoqi Jia, Yi Xing, Liguo Zhang, Wenbo Zhang, Jiaqing Wang et al. Progress of catalytic oxidation of typical chlorined volatile organic compounds (CVOCs): A review. Science of The Total Environment. 2023;865:161063.
3. Zhou, Xihe, Xiang Zhou, Chengming Wang, and Handong Zhou. Environmental and human health impacts of volatile organic compounds: A perspective review. Chemosphere. 2023;313:137489.
4. González-Velasco, J. R., A. Aranzabal, R. López-Fonseca, R. Ferret, and J. A. González-Marcos. Enhancement of the catalytic oxidation of hydrogen-lean chlorinated VOCs in the presence of hydrogen-supplying compounds. Applied Catalysis B: Environmental. 2000;24(1):33-43.
5. Fawei Lin, Zhiman Zhang, Na Li, BeiBei Yan, Chi He et al. How to achieve complete elimination of Cl-VOCs: A critical review on byproducts formation and inhibition strategies during catalytic oxidation. Chemical Engineering Journal. 2021;404:126534.
6. Duan Xiaoxiao, Ting Zhao, Guoxia Jiang, Yingmin Qu, Wenpeng Li. High-

Temperature Catalytic Oxidation of 1,2-Dichlorethane: An Alternative Applicable Method for Safe Elimination of CVOCs. ACS ES&T Engineering. 2022;2(7):1260-1273.

7. Kamal, Muhammad Shahzad, Shaikh A. Razzak, Mohammad M. Hossain. Catalytic oxidation of volatile organic compounds (VOCs)–A review. Atmospheric Environment. 2016;140: 117-134.

8. Xiaoxia Dai, Xinwei Wang, Yunpeng Long, Samuel Pattisson, Yunhao Lu et al. Taylor et al. Efficient elimination of chlorinated organics on a phosphoric acid modified CeO2 catalyst: a hydrolytic destruction route. Environmental Science & Technology. 2019;53(21):12697-12705.

9. Huang Hao, Yufeng Gu, Jian Zhao, Xingyi Wang. Catalytic combustion of chlorobenzene over VOx/CeO2 catalysts. Journal of catalysis. 2015;3 26: 54-68.

10. Yufeng Gu, Ting Cai, Xiaohui Gao, Hangqi Xia, Wei Sun. Catalytic combustion of chlorinated aromatics over WOx/CeO2 catalysts at low temperature. Applied Catalysis B: Environmental. 2019;248 :264-276.

11. Cai, Ting, Hao Huang, Wei Deng, Qiguang Dai, Wei Liu. Catalytic combustion of 1,2-dichlorobenzene at low temperature over Mn-modified Co3O4 catalysts. Applied Catalysis B: Environmental. 2015;166:393-405.

12. Xingyi, Wang, Kang Qian, and Li Dao. Catalytic combustion of chlorobenzene over MnOx–CeO2 mixed oxide catalysts. Applied Catalysis B: Environmental. 2009;86(3-4):166-175.

13. Yim, Sung Dae, and In-Sik Nam. Characteristics of chromium oxides supported on TiO2 and Al2O3 for the decomposition of perchloroethylene. Journal of Catalysis. 2004;221(2): 601-611.

14. Tian Mingjiao Xu Guo, Rui Dong, Zheng Guo, Jianwen Shi et al. Insight into the boosted catalytic performance and chlorine resistance of nanosphere-like meso-macroporous CrOx/MnCo3Ox for 1,2-dichloroethane destruction. Applied Catalysis B: Environmental. 2019;259:118018.

15. Kong, Fanjiao, Chao Wen, Lan Kang, Pin Gao, Lihui Dong Cr2O3 promotes the catalytic performance of Bi-based catalysts for electrochemical CO2 reduction to HCOOH. Molecular Catalysis. 2024;559:114118.

16. Yang Yuying, Meng Guo, and Fuzhen Zhao. Cr2O3 Promoted In2O3 Catalysts for CO2 Hydrogenation to Methanol. ChemPhysChem. 2024;25 (1):e202300530.

17. Huang Y, Tian M, Jiang Z, Ma M, Chen C, Xu H, Zhang J, Albilali R, He C. Inserting Cr2O3 dramatically promotes RuO2/TiO2 catalyst for low-temperature 1,2-dichloroethane deep destruction: Catalytic performance and synergy mechanism. Applied Catalysis B: Environmental. 2022;304:121002.

18. Lu J, Liu J, Zhao Y, He D, Han C, He S, Luo Y. The identification of active chromium species to enhance catalytic behaviors of alumina-based catalysts for sulfur-containing VOC abatement. Journal of hazardous materials. 2020; 384:121289.

19. Krishnamoorthy, Sundaram, Juan A. Rivas, and Michael D. Amiridis. Catalytic oxidation of 1,2-dichlorobenzene over supported transition metal oxides. Journal of Catalysis . 2000;193(2): 264-272.

20. Rotter H, Landau MV, Herskowitz M. Combustion of chlorinated VOC on nanostructured chromia aerogel as catalyst and catalyst support. Environmental Science & Technology. 2005;39(17): 6845-6850.

21. Padilla Ana M., José Corella, and José M. Toledo. Total oxidation of some chlorinated hydrocarbons with commercial chromia based catalysts. Applied Catalysis B: Environmental. 1999;22(2):107-121.

22. Yim Sung Dae, and In-Sik Nam. Characteristics of chromium oxides supported on TiO2 and Al2O3 for the decomposition of perchloroethylene.

Journal of Catalysis. 2004;221(2):601-611.

23. de Rivas, Beatriz, Rubén López-Fonseca, Juan R. González-Velasco, and José I. Gutiérrez-Ortiz. On the mechanism of the catalytic destruction of 1,2-dichloroethane over Ce/Zr mixed oxide catalysts. Journal of Molecular Catalysis A: Chemical. 2007;278(1-2): 181-188.

24. Dai Qiguang, Hao Huang, Yu Zhu, Wei Deng, Shuxing Bai Catalysis oxidation of 1,2-dichloroethane and ethyl acetate over ceria nanocrystals with well-defined crystal planes. Applied Catalysis B: Environmental. 2012;117:360-368.

25. Wang, Xingyi, Qian Kang, and Dao Li. Low-temperature catalytic combustion of chlorobenzene over MnOx–CeO2 mixed oxide catalysts. Catalysis Communications. 2008;9(13):2158-2162.

26. Yang Peng, Zhonghua Meng, Shanshan Yang, Zhinan Shi, Renxian Zhou. Highly active behaviors of CeO2–CrOx mixed oxide catalysts in deep oxidation of 1,2-dichloroethane. Journal of Molecular Catalysis A: Chemical. 2014;393:75-83.

27. Huang, Qinqin, Xiaomin Xue, and Renxian Zhou. Catalytic behavior and durability of CeO2 or/and CuO modified USY zeolite catalysts for decomposition of chlorinated volatile organic compounds. Journal of Molecular Catalysis A: Chemical. 2011;344(1-2):74-82.

28. Dai Qiguang, Shuxing Bai, Jianwei Wang, Meng Li, Xingyi Wang et al. The effect of TiO2 doping on catalytic performances of Ru/CeO2 catalysts during catalytic combustion of chlorobenzene. Applied Catalysis B: Environmental. 2013;142:222-233.

29. Ning Rui, Jingqi Tian, Abdullah M. Asiri, Abdullah H. Qusti, Abdulrahman O. Al-Youbi et al. Spinel CuCo2O4 nanoparticles supported on N-doped reduced graphene oxide: a highly active and stable hybrid electrocatalyst for the oxygen reduction reaction. Langmuir. 2013;29(43):13146-13151.

30. Chen, Shan, Xiudan Liu, Shiyuan Gao, Yanchao Chen, Longjun Rao et al. CuCo2O4 supported on activated carbon as a novel heterogeneous catalyst with enhanced peroxymonosulfate activity for efficient removal of organic pollutants. Environmental Research. 202;183:109245.

31. Ghanbari, Farshid, Mahsa Moradi, and Fariba Gohari. Degradation of 2,4,6-trichlorophenol in aqueous solutions using peroxymonosulfate/activated carbon/UV process via sulfate and hydroxyl radicals. Journal of Water Process Engineering. 2016;9: 22-28.

32. Thommes, Matthias, Katsumi Kaneko, Alexander V. Neimark, James P. Olivier, Francisco Rodriguez-Reinoso et al. Physisorption of gases, with special reference to the evaluation of surface area and pore size distribution (IUPAC Technical Report). Pure and Applied Chemistry. 2015;87(9-10):1051-1069.

33. Cheng, Zhen, Zhu Chen, Jingrong Li, Shufeng Zuo, and Peng Yang. Mesoporous silica-pillared clays supported nanosized Co3O4-CeO2 for catalytic combustion of toluene. Applied Surface Science. 2018;459: 32-39.

34. Zhou Guilin, Xiaoling He, Sheng Liu, Hongmei Xie, Min Fu. Phenyl VOCs catalytic combustion on supported CoMn/AC oxide catalyst. Journal of Industrial and Engineering Chemistry. 2015;21:932-941.

35. Du Jinpeng, Zhenping Qu, Cui Dong, Lixin Song, Yuan Qin. Low-temperature abatement of toluene over Mn-Ce oxides catalysts synthesized by a modified hydrothermal approach. Applied Surface Science. 2018;433: 1025-1035.

36. Venkataswamy Perala, Komateedi N. Rao, Deshetti Jampaiah, and Benjaram M. Reddy. Nanostructured manganese doped ceria solid solutions

for CO oxidation at lower temperatures. Applied Catalysis B: Environmental. 2015;162:122-132.

37. Huang Qinqin, Xiaomin Xue, Renxian Zhou. Decomposition of 1,2-dichloroethane over CeO2 modified USY zeolite catalysts: Effect of acidity and redox property on the catalytic behavior. Journal of Hazardous Materials. 2010;183(1-3):694-700.

38. Lu Han-Feng, Ying Zhou, Wen-Feng Han, Hai-feng Huang, and Yin-Fei Chen. Promoting effect of ZrO2 carrier on activity and thermal stability of CeO2-based oxides catalysts for toluene combustion. Applied Catalysis A: General. 2013;464:101-108.

39. Wang, Xingyi, Qian Kang, Dao Li. Low-temperature catalytic combustion of chlorobenzene over MnOx–CeO2 mixed oxide catalysts. Catalysis Communications. 2008;9(13):2158-2162.

40. Chen, Gong, Dongsen Hong, Hangqi Xia, Wei Sun, Shijie Shao et al. Amorphous and homogeneously Zr-doped MnOx with enhanced acid and redox properties for catalytic oxidation of 1,2-Dichloroethane. Chemical Engineering Journal. 2022;428:131067.

Peer-review history:
The peer review history for this paper can be accessed here:
https://www.sdiarticle5.com/review-history/117025